# Chapter 1
# Introduction

Digital technology has taken over many aspects of our society. From iPod to iPhone, and from eCommerce to eBook, such a digital take over has been one of the most fundamental changes in our time. Although digital take over began at the birth of digital computer, it has been accelerated in the past a few decades by the invention of personal computer (PC) and the development of Internet. Digital technology has conquered us all and changed not only our industry but also our daily life.

This textbook is aimed at covering both the theory and design for linear discrete-time systems built upon the digital technology with applications focusing on feedback control and wireless communications. The material of the book covers from mathematical models of discrete-time signals and systems to design of feedback control systems and wireless transceivers which are fairly extensive and are organized into eight different chapters. In order to help readers' mathematical background, three additional appendix chapters are prepared which make this text quite self-contained. While different opinions exist, it is believed that mathematics can and should be learned together with application examples for at least students in engineering.

Discrete-time/digital systems are originated from the continuous-time/analog world, the world we live in. It is the digital technology that transforms analog systems in continuous time into the digital ones in discrete time with the offer of unprecedented reliability and efficiency in large economic scale. We are compelled to get into the digital world without which we will not be able to compete in the global economy. For this reason, every college student in engineering needs to have some knowledge on linear discrete-time/digital systems. However, this textbook is not for every one. It is prepared for those readers who wish to have more solid theoretical understanding and more advanced design techniques than what they learned in their undergraduate studies. Even though this book can also be used as a text for senior undergraduate students specialized in control or communications, more suitable readers are first and second year graduate students. Because of the technological advances in the past half century, physical systems from controls and communications become increasingly multivariable and involve multi-input and multi-output (MIMO). MIMO systems are more difficult to analyze, and their design

G. Gu, *Discrete-Time Linear Systems: Theory and Design with Applications*,
DOI 10.1007/978-1-4614-2281-5_1, © Springer Science+Business Media, LLC 2012

poses considerable more challenges than single-input/single-output (SISO) systems. This textbook studies MIMO discrete-time systems, their mathematical properties, and various design issues. This introductive chapter presents some MIMO examples arising from controls and communications, and discretization of continuous-time systems.

## 1.1 Control Systems

Control is essential to modern technologies. Without it, there would be no running transportation vehicles in air or on ground or under water and no operating industrial machines, power plants, etc. In one word, no modern technology would function properly without control.

A physical system is a man-made device or machine. Control of the system requires understanding of its properties, its purpose, and its environment. In addition, sensors capable of measuring its state will have to be employed, and actuators capable of adjusting its state will have to be installed. These rough descriptions can all be made precise using mathematics. This section will present several physical processes. Moreover, discretization of continuous-time systems will be investigated in order that digital control can be applied.

### *1.1.1 MIMO Dynamic Systems*

SISO control systems are abundant which can be traced back to ancient Greeks of 2,000 years ago who invented float regulators of water clocks. MIMO feedback control systems have a much shorter history which are the result of insatiable needs of our industry and ultimately our society. Consider an inverted pendulum mounted on a cart that is driven by a motor. See the schematic diagram in Fig. 1.1. The system shares similar dynamics to those of cranes in construction sites and rocket vehicles used in space exploration. Initially, the objective is confined to stabilization of the inverted pendulum by regulating the angle variable $\theta(t)$ to near zero. Later, people began to consider control of the position of the cart in addition to stabilization of the inverted pendulum which makes it a special MIMO system with one input/two output.

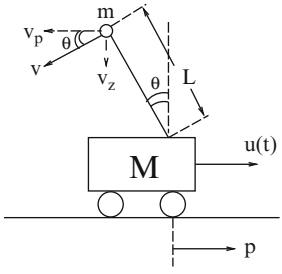


**Fig. 1.1** Inverted pendulum

How can the inverted pendulum be controlled? Our past experience of education and practice in control indicates the necessity of the mathematical model that describes the pendulum-cart dynamics. A commonly adopted approach employs the Lagrange mechanics in modeling that is illustrated with a step by step procedure next.

Step 1 involves computation of the total kinetic energy (KE) of the system. Because of no vertical or rotational movement for the cart,

$$\mathrm{KE}_{\mathrm{cart}} = \frac{1}{2} M \dot{p}^2$$

with $p$ the position of the cart. The KE for the pendulum is found to be

$$\mathrm{KE}_{\mathrm{pen}} = \frac{1}{2} m \left( v_p^2 + v_z^2 \right).$$

In light of the schematic diagram in Fig. 1.1,

$$v_z = L \sin(\theta) \dot{\theta}, \quad v_p^2 = \dot{p}^2 + L^2 \cos^2(\theta) \dot{\theta}^2,$$

due to both rotational and translational movement in $p$ direction. Thus

$$\mathrm{KE}_{\mathrm{pen}} = \frac{1}{2} m \left( \dot{p}^2 + L^2 \dot{\theta}^2 - 2 \dot{p} L \cos(\theta) \dot{\theta} \right).$$

Since the total KE is the sum of $\mathrm{KE}_{\mathrm{cart}}$ and $\mathrm{KE}_{\mathrm{pen}}$, there holds

$$\mathrm{KE} = \frac{1}{2} \left\{ M \dot{p}^2 + m \left( \dot{p}^2 + L^2 \dot{\theta}^2 - 2 \dot{p} L \cos(\theta) \dot{\theta} \right) \right\}.$$

Step 2 computes the total potential energy (PE). Clearly, only the pendulum admits the PE, and thus, $\mathrm{PE} = mgL\cos(\theta)$.

Step 3 forms $L_E = \mathrm{KE} - \mathrm{PE}$, the Lagrange of the system, as

$$L_E = \frac{1}{2} \left\{ M \dot{p}^2 + m \left( \dot{p}^2 + L^2 \dot{\theta}^2 - 2 \dot{p} L \cos(\theta) \dot{\theta} \right) \right\} - mgL\cos(\theta),$$

and then computes the equations of motion in accordance with the following general principle:

$$\frac{\mathrm{d}}{\mathrm{d}t} \left[ \frac{\partial L_E}{\partial \dot{p}} \right] - \left[ \frac{\partial L_E}{\partial p} \right] = u, \tag{1.1}$$

$$\frac{\mathrm{d}}{\mathrm{d}t} \left[ \frac{\partial L_E}{\partial \dot{\theta}} \right] - \left[ \frac{\partial L_E}{\partial \theta} \right] = 0. \tag{1.2}$$

The right-hand side consists of "generalized forces" or external forces corresponding to each degree of freedom: $\theta$ and $p$. The only external force is $u(t)$ applied in direction of $p$. By direct calculations,

$$\begin{aligned}
\frac{\partial L_E}{\partial \theta} &= mL\sin(\theta)\dot{p}\dot{\theta} + mgL\sin(\theta),\\
\frac{\partial L_E}{\partial \dot{\theta}} &= mL^2\dot{\theta} - mL\cos(\theta)\dot{p},\\
\frac{\partial L_E}{\partial p} &= 0, \quad \frac{\partial L_E}{\partial \dot{p}} = (M+m)\dot{p} - mL\cos(\theta)\dot{\theta},\\
\frac{\mathrm{d}}{\mathrm{d}t}\left[\frac{\partial L_E}{\partial \dot{\theta}}\right] &= mL^2\ddot{\theta} - mL\cos(\theta)\ddot{p} + mL\sin(\theta)\dot{\theta}\dot{p},\\
\frac{\mathrm{d}}{\mathrm{d}t}\left[\frac{\partial L_E}{\partial \dot{p}}\right] &= (M+m)\ddot{p} - mL\cos(\theta)\ddot{\theta} + mL\sin(\theta)\dot{\theta}^2.
\end{aligned}$$

Substituting the above into (1.1) and (1.2) gives

$$\begin{aligned}
(M+m)\ddot{p} - mL\cos(\theta)\ddot{\theta} &= u - mL\sin(\theta)\dot{\theta}^2,\\
mL^2\ddot{\theta} - mL\cos(\theta)\ddot{p} &= mgL\sin(\theta),
\end{aligned}$$

which can be written into the matrix form:

$$\begin{bmatrix} -mL\cos(\theta) & M+m \\ mL^2 & -mL\cos(\theta) \end{bmatrix} \begin{bmatrix} \ddot{\theta} \\ \ddot{p} \end{bmatrix} = \begin{bmatrix} u - mL\sin(\theta)\dot{\theta}^2 \\ mgL\sin(\theta) \end{bmatrix}. \tag{1.3}$$

The matrix on left is called inertial matrix, and its determinant is given by

$$\Delta = (M+m)mL^2 - m^2L^2\cos^2(\theta) = (M+m\sin^2(\theta))mL^2. \tag{1.4}$$

Solving $\ddot{\theta}$ and $\ddot{p}$ in (1.3) yields

$$\ddot{\theta} = \frac{mL}{\Delta}\left(\cos(\theta)u - mL\sin(\theta)\cos(\theta)\dot{\theta}^2 + (M+m)g\sin(\theta)\right), \tag{1.5}$$

$$\ddot{p} = \frac{mL^2}{\Delta}\left(u - mL\sin(\theta)\dot{\theta}^2 + mg\sin(\theta)\cos(\theta)\right). \tag{1.6}$$

The three steps as described above are very general that applies not only to modeling of the inverted pendulum but also to modeling of other mechanical systems. The example of inverted pendulum alludes the ordinary different equations (ODEs) in describing the dynamic motions of physical systems. For the inverted pendulum, the ODEs are nonlinear functions of $\theta$ and $p$, but independent of time. For other mechanical systems, the ODE model may depend on time as well. More complex systems may have to be described by partial different equations (PDEs) which are beyond the scope of this text.

In design of MIMO control systems, state-space form of the mathematical model is more convenient. Denote vector by boldfaced letter and $\Longrightarrow$ for "imply." The state vector for the inverted pendulum can be defined as

$$\mathbf{x}(t) = \begin{bmatrix} x_1(t) \\ x_2(t) \\ x_3(t) \\ x_4(t) \end{bmatrix} = \begin{bmatrix} \theta(t) \\ \dot{\theta}(t) \\ p(t) \\ \dot{p}(t) \end{bmatrix} \quad \Longrightarrow \quad \dot{\mathbf{x}}(t) = \mathbf{f}[\mathbf{x}(t)] + \mathbf{g}[\mathbf{x}(t), u(t)]. \tag{1.7}$$

Let $f_i(\mathbf{x})$ and $g_i(\mathbf{x}, u)$ be the $i$th element of $\mathbf{f}(\cdot)$ and $\mathbf{g}(\cdot)$, respectively. It is easy to verify that $f_2(\mathbf{x})$ and $f_4(\mathbf{x})$ are given in (1.6) and (1.5), respectively,

$$f_1(\mathbf{x}) = x_2, \ f_3(\mathbf{x}) = x_4, \ g_1(\mathbf{x}, u) = g_3(\mathbf{x}, u) = 0,$$

and $g_2(\mathbf{x}, u) = mLu\cos(x_1)/\Delta, g_4(\mathbf{x}, u) = mL^2u/\Delta$ with $\Delta$ in (1.4).

In the general case, a MIMO system is described by state-space model of

$$\dot{\mathbf{x}} = \mathbf{f}(t, \mathbf{x}, \mathbf{u}), \ \mathbf{y} = \mathbf{h}(t, \mathbf{x}, \mathbf{u}), \tag{1.8}$$

where $\mathbf{u}$ and $\mathbf{y}$ are input and output vectors, respectively. For the inverted pendulum, input is scalar and output is a vector consisting of $\theta$ and $p$. The argument of $t$ indicates the possible dependence of $\mathbf{f}(\cdot)$ and $\mathbf{h}(\cdot)$ on time.

Control of general nonlinear systems in form of (1.8) is extremely difficult. A tractable approach employs small signal analysis to obtain an approximate linear system prior to design of feedback controllers. This method computes the equilibrium points of $\mathbf{f}(t, \mathbf{x}_e, \mathbf{u}_e) = \mathbf{0}$ first and then chooses some pair of the roots $(\mathbf{x}_e, \mathbf{u}_e)$ as the desired operating point. Selection of $(\mathbf{x}_e, \mathbf{u}_e)$ depends on control objectives, system properties and other possible factors. A first-order approximation can be applied to linearize the system in (1.8). Define

$$A_t = \left.\frac{\partial \mathbf{f}}{\partial \mathbf{x}}\right|_{\mathbf{x}=\mathbf{x}_e, \mathbf{u}=\mathbf{u}_e,} \quad B_t = \left.\frac{\partial \mathbf{f}}{\partial \mathbf{u}}\right|_{\mathbf{x}=\mathbf{x}_e, \mathbf{u}=\mathbf{u}_e,}$$

$$C_t = \left.\frac{\partial \mathbf{h}}{\partial \mathbf{x}}\right|_{\mathbf{x}=\mathbf{x}_e, \mathbf{u}=\mathbf{u}_e,} \quad D_t = \left.\frac{\partial \mathbf{h}}{\partial \mathbf{u}}\right|_{\mathbf{x}=\mathbf{x}_e, \mathbf{u}=\mathbf{u}_e.}$$

Let $\delta\mathbf{x} = \mathbf{x} - \mathbf{x}_e$ and $\delta\mathbf{u} = \mathbf{u} - \mathbf{u}_e$. Then the linear state-space system

$$\delta\dot{\mathbf{x}} = A_t\delta\mathbf{x} + B_t\delta\mathbf{u}, \ \mathbf{y} = C_t\delta\mathbf{x} + D_t\delta\mathbf{u} \tag{1.9}$$

represents a first-order approximation or linearization to the nonlinear system in (1.8). Such an approximation works well for small perturbations. The quadruplet $(A_t, B_t, C_t, D_t)$ is called *realization* of the linearized system.

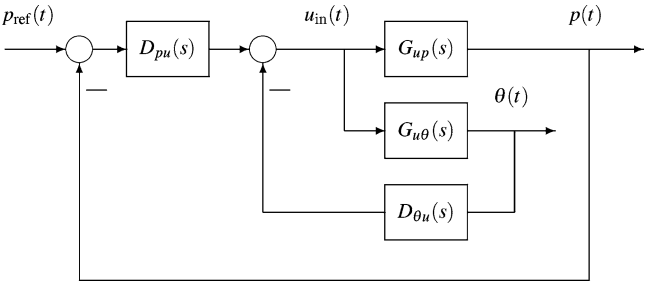


**Fig. 1.2** Feedback control system for inverted pendulum

For inverted pendulum, the equilibrium point of $\mathbf{x}_e = \mathbf{0}$ and $u_e = 0$ is the meaningful one. Carrying out the linearization about the equilibrium point shows that the realization matrices are time invariant given by

$$A = \begin{bmatrix} 0 & 1 & 0 & 0 \\ \frac{(M+m)g}{ML} & 0 & 0 & 0 \\ 0 & 0 & 0 & 1 \\ \frac{mg}{M} & 0 & 0 & 0 \end{bmatrix}, \quad B = \begin{bmatrix} 0 \\ \frac{1}{ML} \\ 0 \\ \frac{1}{M} \end{bmatrix},$$

$$C = \begin{bmatrix} 1 & 0 & 0 & 0 \\ 0 & 0 & 1 & 0 \end{bmatrix}, \qquad D = \begin{bmatrix} 0 \\ 0 \end{bmatrix},$$

by output measurements $x_1 = \theta$ and $x_3 = p$. The inverted pendulum tends to fall down in the case of large signal sizes of $\mathbf{x}(t)$ which is captured by unstable eigenvalues of $A$. The linearized model works well for controlled pendulum in both Matlab simulations and in laboratory experiments.

*Example 1.1.* If the motor dynamics are included, the linearized state-space model has realization matrices given in Problem 1.2 of Exercises. The transfer functions from $u_{\text{in}}$ to $\theta$ and to $p$ can be obtained, respectively, as

$$G_{up}(s) = \frac{\frac{K_m K_g}{MRr}\left(s^2 - \frac{g}{L}\right)}{s\left(s^3 + \frac{K_m^2 K_g^2}{MR r^2}s^2 - \frac{(M+m)g}{ML}s - \frac{gK_m^2 K_g^2}{MLR r^2}\right)},$$

$$G_{u\theta}(s) = \frac{\frac{K_m K_g}{MLRr}s}{s^3 + \frac{K_m^2 K_g^2}{MR r^2}s^2 - \frac{(M+m)g}{ML}s - \frac{gK_m^2 K_g^2}{MLR r^2}}.$$

The block diagram of the pendulum control system is shown in Fig. 1.2. For the laboratory setup of the inverted pendulum system by the Quanzer Inc., the two transfer functions are given, respectively, by

$$G_{up}(s) = \frac{2.4805(s+5.4506)(s-5.4506)}{s(s+12.2382)(s-5.7441)(s+4.7535)}, \tag{1.10}$$

$$G_{u\theta}(s) = \frac{7.512s}{(s+12.2382)(s-5.7441)(s+4.7535)}. \tag{1.11}$$

If the following two simple dynamic compensators

$$D_{pu}(s) = K_{dy}\frac{s+z_y}{s+p_d}, \quad D_{\theta u}(s) = K_{d\theta}\frac{s+z_\theta}{s+p_d}, \tag{1.12}$$

are implemented in feedback block diagram of Fig. 1.2 with parameters specified in Problem 1.3 of Exercises, then the inverted pendulum is stabilized. This example exhibits the resilience of the linearization method. In fact, it is difficult to push down the inverted pendulum by hands in the lab experiment unless excessive forces are exerted to the pendulum.

While the linearization method works well for the control system of the inverted pendulum, it may not work well for other nonlinear control systems because of the large dynamic ranges of the equilibrium points. In this case, a set of linear feedback controllers can be designed for linearized systems at a number of equilibrium points which are then scheduled in operation. The actual controller is an interpolation of several controllers designed for equilibrium points close to the operating point. Such a method is often referred to as *gain schedule* which is widely used. The performance of the gain scheduled system is clearly hinged to that of each linear feedback control system. For this reason, linear systems play a fundamental role in feedback control design that is the focus of this text.

### *1.1.2 System Discretization*

By definition, a discrete-time signal takes its values at only a set of discrete-time samples and is undefined elsewhere. This text considers signal samples taken at only equally spaced time instants. While continuous-time signals are abundant, discrete-time signals are often obtained from discretization of continuous-time ones. The ideal sampler is employed to take samples of the continuous-time signal $s_c(t)$ in accordance with

$$s(k) = s_c(kT_s), \quad k = 0, \pm T_s, \pm 2T_s, \ldots, \tag{1.13}$$

where $T_s > 0$ is the sampling period. Discrete-time signals in practice involve quantization as well that is not addressed in this text.

For a given discrete-time signal $s(k) = s_c(kT_s)$, its frequency response is defined as the discrete-time Fourier transform (DTFT) given by

$$S\left(e^{j\omega}\right) = \mathscr{F}_d[s(k)] := \sum_{k=-\infty}^{\infty} s(k)e^{-jk\omega}. \tag{1.14}$$

A natural question is the relationship between the DTFT and continuous-time Fourier transform (CTFT) defined by

$$S_{\rm c}(j\omega) = \mathscr{F}_{\rm c}[s_{\rm c}(t)] := \int_{-\infty}^{\infty} s_{\rm c}(t) {\rm e}^{-j\omega}\, {\rm d}\omega. \tag{1.15}$$

The Dirac delta function, denoted by $\delta_D(t)$, turns out to be useful. This special function satisfies the following two properties:

$$\text{(i) } \delta_D(t) = 0 \ \forall\, t \neq 0, \quad \text{(ii) } \int_{-\infty}^{\infty} \delta_D(t)\, {\rm d}t = 1. \tag{1.16}$$

It is a continuous-time signal but has some discrete-time flavor by noting that it takes zero value everywhere except at the origin. More importantly, it helps to connect the DTFT and CTFT as shown in the next result.

**Lemma 1.1.** *Denote $\omega_{\rm s} = 2\pi/T_{\rm s}$ as the sampling frequency. The* DTFT *as defined in (1.14) is related to the* CTFT *as defined in (1.15) according to*

$$S\left({\rm e}^{jT_{\rm s}\omega}\right) = \frac{1}{T_{\rm s}} \sum_{k=-\infty}^{\infty} S_{\rm c}(j\omega - jk\omega_{\rm s}). \tag{1.17}$$

*Proof.* Consider the periodic extension of the Dirac delta function

$$p_\delta(t) = \sum_{k=-\infty}^{\infty} \delta_D(t - kT_{\rm s}). \tag{1.18}$$

Its Fourier series expansion is given by

$$p_\delta(t) = \frac{1}{T_{\rm s}} \sum_{i=-\infty}^{\infty} {\rm e}^{-ji\omega_{\rm s}}. \tag{1.19}$$

See Problem 1.4 in Exercises. Let $s_p(t) = s_{\rm c}(t) \times p_\delta(t)$. There holds

$$s_p(t) = \frac{1}{T_{\rm s}} \sum_{k=-\infty}^{\infty} s_{\rm c}(t) {\rm e}^{-jk\omega_{\rm s}t} \tag{1.20}$$

by (1.19). Applying the CTFT to $s_p(t)$ yields

$$\mathscr{F}_{\rm c}[s_p(t)] = \frac{1}{T_{\rm s}} \sum_{k=-\infty}^{\infty} \mathscr{F}_{\rm c}\left[s_{\rm c}(t){\rm e}^{-jk\omega_{\rm s}t}\right] = \frac{1}{T_{\rm s}} \sum_{k=-\infty}^{\infty} S_{\rm c}\left(j\omega - jk\omega_{\rm s}\right) \tag{1.21}$$

by Problem 1.5 in Exercises. On the other hand, there holds

$$s_p(t) = \sum_{k=-\infty}^{\infty} s_{\rm c}(kT_{\rm s})\delta_D(t - kT_{\rm s}) = \sum_{k=-\infty}^{\infty} s(k)\delta_D(t - kT_{\rm s}). \tag{1.22}$$

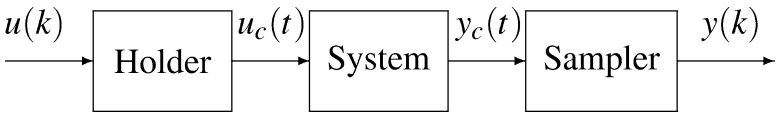


**Fig. 1.3** Discretization with zero-order holder and ideal sampler

Hence applying the CTFT to $s_p(t)$ yields

$$\mathscr{F}_{\mathrm{c}}[s_p(t)] = \sum_{k=-\infty}^{\infty} s(k)\mathrm{e}^{-jkT_{\mathrm{s}}\omega} = S\left(\mathrm{e}^{jT_{\mathrm{s}}\omega}\right). \tag{1.23}$$

The proof is complete. □

The well-known sampling theorem can be derived based on Lemma 1.1 by noting that $S(\mathrm{e}^{jT_{\mathrm{s}}\omega})$ consists of a train of shifted images of $S_{\mathrm{c}}(j\omega)$. Hence, if $S_{\mathrm{c}}(j\omega)$ admits low-pass characteristic, i.e., $|S_{\mathrm{c}}(j\omega)|$ is symmetric about $\omega = 0$ and admits finite cut-off frequency $\omega_{\mathrm{c}} < \omega_{\mathrm{s}}/2$, then the train of shifted images of $S_{\mathrm{c}}(j\omega)$ in (1.17) does not overlap. In practice, $\omega_{\mathrm{c}}$ is taken as the first frequency beyond which the magnitude response $|S_{\mathrm{c}}(j\omega)|$ falls within 3% of its peak.

Discretization of the continuous-time system takes more than the ideal sampler at the plant output. A zero-order holder is often employed at the plant input to convert the discrete-time signal into the continuous-time one. See the block diagram in Fig. 1.3. The zero-order holder is mathematically defined by

$$u_{\mathrm{c}}(t) = u(k),\ kT_{\mathrm{s}} \le t < (k+1)T_{\mathrm{s}}, \tag{1.24}$$

where $k = 0, \pm 1, \pm 2, \ldots$. The above can also be written as

$$u_{\mathrm{c}}(t) = \sum_{k=-\infty}^{\infty} u(k)\left[\mathbf{1}(t - kT_{\mathrm{s}}) - \mathbf{1}(t - T_{\mathrm{s}} - kT_{\mathrm{s}})\right], \tag{1.25}$$

where $\mathbf{1}(t)$ is the unit step function specified by

$$\mathbf{1}(t) = \begin{cases} 1, & t \ge 0, \\ 0, & t < 0. \end{cases} \tag{1.26}$$

Hence, the continuous-time signal at the output of the holder consists of piecewise constants and may have discontinuity at each sampling instant. The following result presents characterization of the zero-order holder. The proof is left as an exercise (Problem 1.6).

**Lemma 1.2.** *For the ideal holder defined in (1.24), there holds*

$$U_{\mathrm{c}}(j\omega) = R(j\omega)U\left(\mathrm{e}^{jT_{\mathrm{s}}\omega}\right),\ R(j\omega) = \left(\frac{1 - \mathrm{e}^{-jT_{\mathrm{s}}\omega}}{j\omega}\right). \tag{1.27}$$

The discretization shown in Fig. 1.3 is also referred to as step-invariant transform (SIT), because it preserves the step response in the sense that its step response is sampling of the step response of the corresponding continuous-time system. This is shown in the next result.

**Theorem 1.2.** *Let $G(s)$ be the transfer function of the continuous-time system and $G_d(z)$ be the transfer function for the corresponding discretized system in Fig. 1.3. Then there holds*

$$G_d\left(\mathrm{e}^{j\omega}\right) = \sum_{k=-\infty}^{\infty} G(j\omega + jk\omega_\mathrm{s})R(j\omega + jk\omega_\mathrm{s}). \tag{1.28}$$

*Proof.* In reference to Fig. 1.3 and in light of Lemma 1.2, there holds

$$Y_\mathrm{c}(j\omega) = G(j\omega)U_\mathrm{c}(j\omega) = G(j\omega)R(j\omega)U\left(\mathrm{e}^{jT_\mathrm{s}\omega}\right).$$

The discretized signal after the ideal sampler is $y(k) = y_\mathrm{c}(kT_\mathrm{s})$, and thus

$$Y(\mathrm{e}^{j\omega}) = \sum_{k=-\infty}^{\infty} Y_\mathrm{c}(j\omega + jk\omega_\mathrm{s}) = \sum_{k=-\infty}^{\infty} G(j\omega + jk\omega_\mathrm{s})R(j\omega + jk\omega_\mathrm{s})U\left(\mathrm{e}^{jT_\mathrm{s}\omega}\right)$$

by the periodicity of $U\left(\mathrm{e}^{jT_\mathrm{s}\omega}\right)$ with $\omega_\mathrm{s} = 2\pi/T_\mathrm{s}$ as the period and in light of Lemma 1.1. Hence, (1.28) holds that concludes the proof. □

Again, by the periodicity of $\mathrm{e}^{jT_\mathrm{s}\omega}$ with $\omega_\mathrm{s}$ as the period, the step response of the discretized system in frequency domain is given by

$$Y_\mathrm{s}\left(\mathrm{e}^{jT_\mathrm{s}\omega}\right) = \frac{G_d\left(\mathrm{e}^{jT_\mathrm{s}\omega}\right)}{1-\mathrm{e}^{-jT_\mathrm{s}\omega}} = \sum_{k=-\infty}^{\infty} \frac{G(j\omega + jk\omega_\mathrm{s})}{j\omega + jk\omega_\mathrm{s}}. \tag{1.29}$$

The right-hand side is the step response of the continuous-time system after the ideal sampling by Lemma 1.1. Hence, the discretization in Fig. 1.3 is indeed SIT and preserves the step response. Next, a numerical procedure is presented for computing the discretized system in Fig. 1.3 based on state-space models.

Consider the MIMO continuous-time state–space system described by

$$\dot{\mathbf{x}}(t) = A\mathbf{x}(t) + B\mathbf{u}(t),\ \mathbf{y}(t) = C\mathbf{x}(t) + D\mathbf{u}(t).$$

It is known that for any $t_2 > t_1$, there holds

$$\mathbf{x}(t_2) = e^{A(t_2-t_1)}\mathbf{x}(t_1) + \int_{t_1}^{t_2} e^{A(t_2-t_1)}B\mathbf{u}(\tau)\,\mathrm{d}\tau.$$

Taking $t_1 = kT_\mathrm{s}$, and $t_2 = (k+1)T_\mathrm{s}$ yields

$$\mathbf{x}[(k+1)T_\mathrm{s}] = e^{Ah}\mathbf{x}(kT_\mathrm{s}) + \int_{kT_\mathrm{s}}^{(k+1)T_\mathrm{s}} e^{A[(k+1)T_\mathrm{s}-\tau]}B\mathbf{u}(\tau)\,\mathrm{d}\tau.$$

If a zero-order holder is employed at the input, then $\mathbf{u}(t) = \mathbf{u}(kT_\mathrm{s})$ for $kT_\mathrm{s} \le t < (k+1)T_\mathrm{s}$, and thus

$$\begin{aligned}\mathbf{x}[(k+1)T_\mathrm{s}] &= e^{AT_\mathrm{s}}\mathbf{x}(kT_\mathrm{s}) + \int_0^{T_\mathrm{s}} e^{A\tau}\,\mathrm{d}\tau B\mathbf{u}(kT_\mathrm{s}) \\ &= A_d\mathbf{x}(kT_\mathrm{s}) + B_d\mathbf{u}(kT_\mathrm{s}).\end{aligned}$$

The ideal sampling at the output yields

$$\mathbf{y}(kT_\mathrm{s}) = C\mathbf{x}(kT_\mathrm{s}) + D\mathbf{u}(kT_\mathrm{s}).$$

Hence, under SIT, a realization of the continuous-time system is mapped to a realization $(A_d, B_d, C, D)$ for the discretized state-space system where

$$A_d = e^{AT_\mathrm{s}},\ B_d = \int_0^{T_\mathrm{s}} e^{A\tau}\,\mathrm{d}\tau B. \tag{1.30}$$

If $|A| \neq 0$, then $B_d = A^{-1}(e^{AT_\mathrm{s}} - I)B$. Although discretization was discussed for SISO systems earlier, the above shows that SIT is applicable to MIMO systems by employing the zero-order holder in each of the input channels and the ideal sampler in each of the output channels.

*Example 1.3.* Consider $G(s) = \frac{1}{s^3}$. It admits a realization $(A,B,C,D)$ with $C = \begin{bmatrix}1 & 0 & 0\end{bmatrix}$, $D = 0$, and

$$A = \begin{bmatrix}0 & 1 & 0\\ 0 & 0 & 1\\ 0 & 0 & 0\end{bmatrix},\quad B = \begin{bmatrix}0\\ 0\\ 1\end{bmatrix}.$$

Since $A^3 = 0$, it is nilpotent. So for $T_\mathrm{s} = h > 0$,

$$A_d = e^{Ah} = I + Ah + \frac{A^2h^2}{2} = \begin{bmatrix}1 & h & h^2/2\\ 0 & 1 & h\\ 0 & 0 & 1\end{bmatrix},$$

$$B_d = \int_0^h \left(I + A\tau + \frac{A^2\tau^2}{2}\right)\mathrm{d}\tau B = \begin{bmatrix}h^3/3!\\ h^2/2!\\ h\end{bmatrix}.$$

Via direct calculations, it can be verified that

$$G_d(z) = C(zI - A_d)^{-1}B_d = \frac{h^3(z^2+4z+1)}{3!(z-1)^3}. \tag{1.31}$$

Matlab command $[A_d, B_d] = \mathrm{c2d}(A,B,h)$ can be used to obtain numerical values of $(A_d, B_d)$ for a given $h > 0$.

Discretization under SIT can also be carried out directly for transfer function models that is given in the following result.

**Corollary 1.1.** *Assume that $G(s)$ is strictly proper. Then under the same hypothesis of Theorem 1.2, there holds*

$$G_d(z) = (1 - z^{-1})\mathrm{Res}\left[\frac{e^{sT_\mathrm{s}}z^{-1}}{1 - z^{-1}e^{sT_\mathrm{s}}}\frac{G(s)}{s}\right], \tag{1.32}$$

*where* $\mathrm{Res}[\,\cdot\,]$ *denotes operation of residues computed at poles of* $\frac{1}{s}G(s)$.

*Proof.* In light of (1.29), the proof amounts to showing

$$Y_\mathrm{s}\left(e^{jT_\mathrm{s}\omega}\right) = \sum_{k=-\infty}^{\infty}\frac{G(j\omega + jk\omega_\mathrm{s})}{j\omega + jk\omega_\mathrm{s}} = \mathrm{Res}\left[\frac{e^{sT_\mathrm{s}}z^{-1}}{1 - z^{-1}e^{sT_\mathrm{s}}}\frac{G(s)}{s}\right] \tag{1.33}$$

at $z = \mathrm{e}^{jT_\mathrm{s}\omega}$. By the inverse Laplace transform,

$$y_\mathrm{s}(k) = \frac{1}{2\pi j}\int_{\sigma - j\infty}^{\sigma + j\infty}\frac{G(s)}{s}e^{skT_\mathrm{s}}\,\mathrm{d}s$$

for $k \geq 1$ by strict proper $G(s)$. Hence, for $\left|e^{sT_\mathrm{s}}z^{-1}\right| < 1$, there holds

$$\begin{aligned} Y_\mathrm{s}(z) &= \sum_{k=1}^{\infty}y_\mathrm{s}(k)z^{-k} = \frac{1}{2\pi j}\int_{\sigma - j\infty}^{\sigma + j\infty}\frac{G(s)}{s}\sum_{k=1}^{\infty}e^{skT_\mathrm{s}}z^{-k}\mathrm{d}s \\ &= \frac{1}{2\pi j}\int_{\sigma - j\infty}^{\sigma + j\infty}\frac{e^{sT_\mathrm{s}}z^{-1}}{1 - z^{-1}e^{sT_\mathrm{s}}}\frac{G(s)}{s}\,\mathrm{d}s. \end{aligned} \tag{1.34}$$

The relative degree of at least two for $\frac{1}{s}G(s)$ implies that

$$Y_\mathrm{s}(z) = \frac{1}{2\pi j}\oint_{\Gamma_-}\frac{e^{sT_\mathrm{s}}z^{-1}}{1 - z^{-1}e^{sT_\mathrm{s}}}\frac{G(s)}{s}\,\mathrm{d}s, \tag{1.35}$$

where $\Gamma_-$ is the closed contour consisting of the vertical line $s = \sigma + j\omega$ for $\omega \in (-\infty, \infty)$ and the semicircle to the left of the vertical line. Hence, (1.33) holds that completes the proof. □

*Example 1.4.* Consider discretization of $G(s) = \frac{1}{s^3}$ using Corollary 1.1 with $T_\mathrm{s} = h > 0$. Then $\frac{G(s)}{s} = \frac{1}{s^4}$, and thus

$$G_d(z) = \frac{z - 1}{z}\mathrm{Res}\left[\frac{e^{sh}}{z - e^{sh}}\frac{1}{s^4}\right] \tag{1.36}$$

where the residue is computed at $s = 0$ with multiplicity 4. It follows that

$$G_d(z) = \frac{z-1}{3!z} \frac{\mathrm{d}^3 f(s)}{\mathrm{d}s^3}\bigg|_{s=0}, \quad f(s) = \frac{e^{sh}}{z - e^{sh}}. \tag{1.37}$$

Direct calculation shows that

$$\begin{aligned}
\frac{\mathrm{d}f(s)}{\mathrm{d}s} &= \frac{hz^2}{(z-e^{sh})^2} - \frac{hz}{z-e^{sh}}, \\
\frac{\mathrm{d}^2 f(s)}{\mathrm{d}s^2} &= \frac{2h^2 z^3}{(z-e^{sh})^3} - \frac{h^2 e^{sh} z}{(z-e^{sh})^2}, \\
\frac{\mathrm{d}^3 f(s)}{\mathrm{d}s^3}\bigg|_{s=0} &= \frac{6h^3 z^3}{(z-1)^4} - \frac{6h^3 z^2}{(z-1)^3} + \frac{h^3 z}{(z-1)^2}.
\end{aligned}$$

After substituting the above into (1.37) yields

$$G_d(z) = \frac{h^3(z^2+4z+1)}{3!(z-1)^3}$$

that is identical to the expression in (1.31).

A consequence of the SIT discretization is the nonminimum phase system under the high sampling frequency as shown next.

**Corollary 1.2.** *Consider SIT discretization for the continuous-time system represented by its transfer function $G(s)$ that has relative degree $\ell \geq 2$. Then as the sampling period $T_\mathrm{s} \to 0$, $(\ell - 1)$ zeros of $G_d(z)$ tend to be unstable.*

*Proof.* Under the SIT, the $\mathscr{Z}$ transform of the discretized step response is given in (1.34). Instead of closing the contour to the left as in the proof of Corollary 1.1, consider closing contour to the right of $s = \sigma$, where $\sigma$ is real and all poles of $\frac{1}{s}G(s)$ locate on left of $s = \sigma$. Recall that the relative degree $\ell \geq 2$. Hence, (1.35) is now replaced by

$$Y_\mathrm{s}(z) = \frac{1}{2\pi j} \oint_{\Gamma_+} \frac{e^{sT_\mathrm{s}} z^{-1}}{1 - z^{-1} e^{sT_\mathrm{s}}} \frac{G(s)}{s}\, \mathrm{d}s, \tag{1.38}$$

where $\Gamma_+$ is the closed contour consisting of the vertical line $s = \sigma + j\omega$ for $\omega \in (-\infty, \infty)$ and the semicircle to the right of the vertical line. As a result, the residues associated with the above contour integral are those due to roots of $z = e^{sT_\mathrm{s}}$, i.e.,

$$s_k = (\log(z) + j2k\pi)/T_\mathrm{s}, \quad k = 0, \pm 1, \ldots.$$

Hence, in this case, by employing the L'Hospital's rule,

$$G_d(z) = \frac{1 - z^{-1}}{T_\mathrm{s}} \sum_{k=-\infty}^{\infty} \frac{G(s_k)}{s_k}.$$

Note that if $T_s \approx 0$, then $s_k \approx \infty$. For the given $G(s)$, it has the form

$$G(s) = \frac{(s-z_1)\cdots(s-z_m)}{(s-p_1)\cdots(s-p_n)},$$

with relative degree $\ell = n-m \geq 2$. Let $G_1(s) = s^{-\ell}$ and

$$G_2(s) = \frac{s^\ell(s-z_1)\cdots(s-z_m)}{(s-p_1)\cdots(s-p_n)} \implies G_2(\infty) = 1.$$

Now take $|z-1| \geq \delta > 0$ with $\delta \approx 0$, and $|z| \geq 1$. Then

$$\begin{aligned} G_d(z) &= \frac{1-z^{-1}}{T_s} \sum_{k=-\infty}^{\infty} \frac{G_1(s_k)G_2(s_k)}{s_k} \\ &\approx \frac{1-z^{-1}}{T_s} \sum_{k=-\infty}^{\infty} \frac{G_1(s_k)}{s_k} = G_{1d}(z), \end{aligned}$$

where $G_2(s_k) \approx G_2(\infty) = 1$ for each $k$. Since $G_{1d}(z)$ is discretization of $s^{-\ell}$, it has the form

$$G_{1d}(z) = \frac{T_s^\ell z^{-1}\alpha_\ell(z)}{(1-z^{-1})^\ell}, \quad \alpha_\ell(z) = \sum_{i=0}^{\ell} \alpha_i z^{-i},$$

which has unstable roots for $\ell \geq 2$. The case with $\ell = 3$ is given in Example 1.3 in which $\alpha_\ell(z)$ indeed has unstable roots. □

Traditionally, SIT is associated with discretization of continuous-time systems based on which discrete-time feedback controllers are designed and implemented. However, continuous-time controllers are sometime designed first and discretized later prior to their implementation. Although SIT can be used, one may wish to preserve the frequency response, rather than step response, of the feedback controller. This gives rise to the bilinear transform (BT) method for discretization.

Let $T_s$ be the sampling period. Consider approximation of integral $\frac{1}{s}$:

$$\begin{aligned} y(kT_s + T_s) &= y(kT_s) + \int_{kT_s}^{(k+1)T_s} u(\tau)\, \mathrm{d}\tau \\ &= y(kT_s) + 0.5h[u(kT_s) + u(kT_s + T_s)]. \end{aligned}$$

Applying the $\mathscr{Z}$ transform to the above difference equation yields

$$\frac{Y(z)}{U(z)} = \frac{T_s}{2}\left(\frac{z+1}{z-1}\right) \implies s \approx \frac{2}{T_s}\left(\frac{z-1}{z+1}\right).$$

The above leads to the BT for discretization:

$$G_{\rm bt}(z) = G\left(\gamma\frac{z-1}{z+1}\right),\ \gamma = \frac{2}{T_{\rm s}}. \tag{1.39}$$

If $G(s)$ has realization $(A,B,C,D)$ and $\gamma$ is not an eigenvalue of $A$, then

$$\begin{aligned} A_{\rm bt} &= (\gamma I + A)(\gamma I - A)^{-1}, B_{\rm bt} = \sqrt{2\gamma}(\gamma I - A)^{-1}B, \\ C_{\rm bt} &= \sqrt{2\gamma}C(\gamma I - A)^{-1}, D_{\rm bt} = D + C(\gamma I - A)^{-1}B, \end{aligned} \tag{1.40}$$

are realization matrices for $G_{\rm bt}(z)$. The verification of the above expressions is left as an exercise (Problem 1.7).

*Example 1.5.* Consider first $G(s) = \frac{1}{s+1}$. Then the discretized transfer function based on BT is given by

$$\begin{aligned} G_{\rm bt}(z) &= \frac{1}{\gamma\left(\frac{z-1}{z+1}\right)+1} = \frac{z+1}{\gamma(z-1)+(z+1)} \\ &= \frac{z+1}{(\gamma+1)z-(\gamma-1)} = \frac{1}{\gamma+1}\frac{z+1}{z-\frac{\gamma-1}{\gamma+1}}. \end{aligned}$$

Substituting the relation $\gamma = \frac{2}{T_{\rm s}}$ yields

$$G_{\rm bt}(z) = \frac{T_{\rm s}}{2+T_{\rm s}}\frac{z+1}{z-\frac{2-T_{\rm s}}{2+T_{\rm s}}}. \tag{1.41}$$

If the SIT method is used to discretize $G(s)$, then by noting the poles of $\frac{1}{s}G(s)$ at $0,-1$, and in light of Corollary 1.1, there holds

$$\begin{aligned} G_d(z) &= \left(1-z^{-1}\right)\text{Res}\left[\frac{e^{sT_{\rm s}}z^{-1}}{1-z^{-1}e^{sT_{\rm s}}}\frac{G(s)}{s}\right]\Bigg|_{s=0,-1} \\ &= \frac{(1-z^{-1})e^{sT_{\rm s}}z^{-1}}{(s+1)(1-e^{sT_{\rm s}}z^{-1})}\Bigg|_{s=0} + \frac{(1-z^{-1})e^{sT_{\rm s}}z^{-1}}{s(1-e^{sT_{\rm s}}z^{-1})}\Bigg|_{s=-1} \\ &= z^{-1} - \frac{(1-z^{-1})e^{-T_{\rm s}}z^{-1}}{1-e^{-T_{\rm s}}z^{-1}} = \frac{1-e^{-T_{\rm s}}}{z-e^{-T_{\rm s}}}. \end{aligned}$$

Clearly, $G_{\rm bt}(z)$ and $G_d(z)$ are very different from each other.

While SIT-based discretization involves frequency distortion, it preserves step response. On the other hand, the BT-based discretization involves both frequency distortion and step response distortion. Specifically under the BT, the discretized frequency response is given by

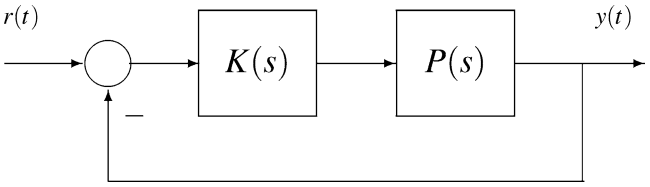


**Fig. 1.4** Feedback control system in continuous time

$$G_{\mathrm{bt}}\left(\mathrm{e}^{j\omega}\right) = G\left(j\frac{2}{T_{\mathrm{s}}}\tan\frac{\omega T_{\mathrm{s}}}{2}\right).$$

The distortion is caused by the nonlinear map in frequency termed as *frequency warping*. It is interesting to note that if $\omega_{\mathrm{c}} = \frac{2}{T_{\mathrm{s}}}\tan\frac{\omega T_{\mathrm{s}}}{2}$ were the continuous-time frequency, then there would be no error in frequency domain. The error in frequency response is given by

$$\left|G(j\omega) - G\left(j\frac{2}{T_{\mathrm{s}}}\tan\frac{\omega T_{\mathrm{s}}}{2}\right)\right|$$

which is zero at $\omega = 0$. The error at other frequencies is caused by frequency warping. The frequency warping can be avoided at $\omega = \omega_0 \neq 0$, if

$$s \mapsto \omega_0\left(\tan\frac{\omega_0 T_{\mathrm{s}}}{2}\right)^{-1}\frac{z-1}{z+1}$$

is used for BT-based discretization, in which case the frequency response at $\omega = \omega_0$ is preserved. This is the so-called frequency-prewarping BT.

Although the BT is different from the SIT in discretizing the continuous-time system, its implementation can be the same in the sense of the block diagram in Fig. 1.3 by using the zero-order holder and ideal sampler for the plant model. That is, the discrete-time controller is obtained via the BT based on the continuous-time controller and is implemented to control the discretized plant in Fig. 1.3. Since in this case the continuous-time controllers are often designed using the frequency domain technique, caution needs to be taken in frequency prewarping. For instance, one may wish to preserve the phase margin or gain margin of the continuous-time feedback system at certain critical frequency by using the frequency prewarping. However, because the frequency response of the discretized plant in Fig. 1.4 is altered (see Problem 1.8 in Exercises for the ideal case), the design of the continuous-time controller in frequency domain needs to take the frequency response error of the plant into consideration so that the phase margin or gain margin of the continuous-time feedback system at the chosen critical frequency can indeed be preserved.

*Example 1.6.* Consider the same transfer function $P(s) = \frac{1}{s+1}$ as in Example 1.5 for the plant model. An integral controller with $K(s) = \frac{\sqrt{2}}{s}$ in continuous time

is designed that achieves the phase margin of 45° at the crossover frequency $\omega_0 = 1$ radian per second. The feedback control system in continuous time is shown in Fig. 1.4. The BT is used to discretize the continuous-time controller for its implementation in discrete time, while the SIT is employed to discretize the plant yielding

$$P_d(z) = \frac{1 - e^{-T_s}}{z - e^{-T_s}},\ K_d(z) = \left(\tan\frac{T_s}{2}\right)\frac{z+1}{z-1},$$

where the frequency prewarping at $\omega_0 = 1$ is employed. If $T_s = 0.25$ is taken, i.e., the sampling frequency is 4 Hz, then the gain of $|P(j\omega_s/2)|$ is $-22$ dB at half the sampling frequency. Hence, possible aliasing due to sampling of the plant is suppressed significantly. However, $\left|K_d\left(\mathrm{e}^{j\omega}\right)P_d\left(\mathrm{e}^{j\omega}\right)\right| = 1$ takes place at $\omega_1 = 0.786$ rather than at $\omega_0 = 1$. If the gain of $K_d(z)$ is increased to assure the crossover frequency at 1 for the discretized feedback system, then the phase margin will be reduced to 37.54°. On the other hand, if 45° phase margin is required for the discretized feedback system, then the crossover frequency has to be smaller than 1, unless a more complicated controller is used.

Before ending this subsection, let us briefly discuss the pathological sampling as illustrated in the following example.

*Example 1.7.* Let $T_s$ be the sampling period. Consider

$$G(s) = \frac{\omega_s s}{s^2 + \omega_s^2},\ \omega_s = \frac{2\pi}{T_s}.$$

With step input $U(s) = 1/s$, the output of the plant is

$$Y(s) = G(s)U(s) = \frac{\omega_s}{s^2 + \omega_s^2} \implies y(t) = \sin(\omega_s t).$$

Hence, the sampling yields $y(kh) = 0$ for all integer-valued $k$. This is so-called pathological sampling. Note that $G(s)$ admits a realization:

$$G(s) = \left[\begin{array}{c|c} A & B \\ \hline C & D \end{array}\right] = \left[\begin{array}{cc|c} 0 & 1 & 0 \\ -\omega_s^2 & 0 & 1 \\ \hline 0 & \omega_s & 0 \end{array}\right],$$

and thus, $A$ has eigenvalues at $\pm j\omega_s$. It can be verified that

$$A_d = e^{Ah} = \begin{bmatrix} \cos(2\pi) & \omega_s^{-1}\sin(2\pi) \\ -\omega_s \sin(2\pi) & \cos(2\pi) \end{bmatrix} = I,$$

$$B_d = \int_0^h e^{At} B\, \mathrm{d}t = A^{-1}[e^{Ah} - I] = 0.$$

Hence, sampling destroys the controllability.

**Definition 1.1.** The sampling frequency $\omega_s$ is pathological, if $A$ or poles of the plant model has two eigenvalues with equal real parts and imaginary parts that differ an integral multiple of $\omega_s$. Otherwise, the sampling frequency $\omega_s$ is called nonpathological.

The pathological can be easily avoided by taking the sampling frequency strictly greater than $\rho(A)$, the spectral radius of $A$. In fact, the sampling frequency smaller or equal to $\rho(A)$ causes the aliasing which should be avoided.

## 1.2 Communication Systems

Communication has enjoyed tremendous growth in the past century. The telephones invented by Bell have grown into communication networks and are now transformed into wireless handheld devices which can surf internet, play videos, and connect to computer networks. An important application content of this text focuses on design of wireless transceivers which are the building block and the physical layer of the wireless networks.

A digital communication system is linear and operates in discrete time. Its purpose lies in communication of digital data or symbols which have finite alphabet table. These data cannot be transmitted and received directly. They have to be modulated with continuous-time waveforms and converted to radio frequency (RF) signals prior to transmission and reception, leading to linear discrete-time systems for wireless data communications. A mathematical description is outlined next without providing the full detail.

### *1.2.1 Channel Models*

Let $\tilde{s}(t)$ be the continuous-time waveforms carrying the data information. Its frequency response exhibits low-pass property normally which is often referred to as baseband signal. The RF signal to be transmitted has the form

$$s(t) = \text{Real}\left[e^{j\omega_c t}\tilde{s}(t)\right], \tag{1.42}$$

where $\omega_c$ is the carrier frequency and $\tilde{s}(t)$ is the complex envelope of the transmitted signal. Thus, the RF signal $s(t)$ admits bandpass property. Let $\tilde{s}(t) = \tilde{s}_I(t) + j\tilde{s}_Q(t)$ with $\tilde{s}_I(t)$ the real or in-phase part and $\tilde{s}_Q(t)$ the imaginary or quadrature part of the envelope signal. Simple calculation shows

$$s(t) = \cos(\omega_c t)\tilde{s}_I(t) - \sin(\omega_c t)\tilde{s}_Q(t).$$

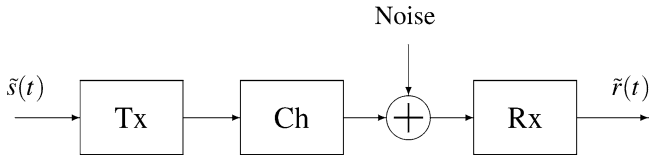


**Fig. 1.5** Baseband signal model with Tx for transmitter and Rx for receiver antennas

Since $\cos(\omega_c t)$ and $\sin(\omega_c t)$ are orthogonal over the period $T_c = \frac{\omega_c}{2\pi}$, $\tilde{s}(t)$ can be reconstructed uniquely based on $s(t)$. Indeed, the in-phase component of $\tilde{s}(t)$ can be obtained by multiplying $s(t)$ with $\cos(\omega_c t)$ and by integration over $[0,\ T_c]$ in light of the fact that $\tilde{s}(t)$ is almost constant over $[0,\ T_c]$ due to the low-pass property of $\tilde{s}(t)$ and very high value of $\omega_c$. Similarly, the quadrature component of $\tilde{s}(t)$ can be obtained by multiplying $s(t)$ with $-\sin(\omega_c t)$ and by the same integration. Consequently, $s(t)$ and $\tilde{s}(t)$ are equivalent in terms of communication.

Assume vertical polarization, plane waves, and $N$ propagation paths for the RF signal transmitted over the space. The received signal in the $k$th path may experience magnitude distortion $C_k$, time delay $d_k$, and Doppler shift $\omega_{D,k}$ (that is positive if the motion is in the direction of the plane waves). Hence, the RF signal at the receiver in absence of the noise is specified by

$$r(t) = \sum_{k=1}^{N} \text{Real}\left[C_k \mathrm{e}^{j(\omega_c+\omega_{D,k})(t-d_k)} \tilde{s}(t-d_k)\right]. \tag{1.43}$$

Let $\phi_k(t) = \omega_c d_k - \omega_{D,k}(t-d_k)$. Then $r(t) = \text{Real}\left[\mathrm{e}^{j\omega_c t}\tilde{r}(t)\right]$ is in the same form of (1.42). The received complex envelope can find to be

$$\tilde{r}(t) = \sum_{k=1}^{N} C_k e^{-j\phi_k(t)} \tilde{s}(t-d_k). \tag{1.44}$$

The above baseband signal can be obtained by first multiplying $\mathrm{e}^{-j\omega_c t}$ to the RF signal $r(t)$ in the receiver's antenna and then by filtering with a low-pass analog filter tailored to $\tilde{r}(t)$. The aforementioned discussions lead to the conclusion that there is no loss of generality to consider data communications in baseband with complex envelope signals as illustrated in Fig. 1.5 next.

The expression in (1.44) shows that the channel can be modeled by a linear time-varying (LTV) system with the complex impulse response:

$$g(t;\tau) = \sum_{k=1}^{N} C_k e^{-j\phi_k(t)} \delta_D(\tau - d_k). \tag{1.45}$$

See Problem 1.12 in Exercises. Recall that $\delta_D(\cdot)$ is the Dirac delta function satisfying (1.16). Under the impulse response in (1.45), the output $y(t)$ due to input $\tilde{s}(t)$ has the following expression:

$$y(t) = \int_{-\infty}^{\infty} g(t; t-\tau)\tilde{s}(\tau)\, \mathrm{d}\tau. \tag{1.46}$$

Hence, $g(t;\tau)$ is interpreted as the impulse response at time $t$ due to the impulse input applied at time 0.

A channel represented by its impulse response in (1.45) suffers from both magnitude attenuation and phase distortion which are generally referred to as channel fading. Denote the duration of a modulated symbol by $T_s$. If $T_s \gg |d_i - d_k|$ for each pair of $(i,k)$, then all frequency components of the transmitted signal experience the same random attenuation and phase shift due to multipath fading. Let $\mu_d$ be the mean of $\{d_k\}$. Then multipath delay spreads fluctuate about $\mu_d$ and

$$g(t;\tau) \approx \sum_{k=1}^{N} C_k e^{-j\phi_k(t)} \delta_D(\tau - \mu_d) = g(t)\delta_D(\tau - \mu_d). \tag{1.47}$$

In this case, the channel experiences flat fading and can be characterized by transmission of an unmodulated carrier. For this reason, $\tilde{s}(t) = 1$ can be assumed for (1.42), and $r(t)$ in (1.43) can be expressed as

$$r(t) = g_I(t)\cos(\omega_c t) - g_Q(t)\sin(\omega_c t), \tag{1.48}$$

where $g_I(t)$ and $g_Q(t)$ are the in-phase and quadrature components of the received signal, respectively, specified by

$$g_I(t) = \sum_{k=1}^{N} C_k \cos[\phi_k(t)],\ g_Q(t) = \sum_{k=1}^{N} C_k \sin[\phi_k(t)]. \tag{1.49}$$

The carrier frequency is often very high for data communications. Hence, small changes of the path delays $\{d_k\}$ will cause large variations in the phases $\{\phi_k(t)\}$ due to the terms $\omega_c d_k \gg 1$. At each time instant $t$, the random phases may result in constructive or destructive addition of the $N$ multipath components. Consequently, $\phi_i(t)$ and $\phi_k(t)$ can be treated as uncorrelated random variables whenever $i \neq k$. It follows that for large $N$, $g_I(t)$ and $g_Q(t)$ are independent and approximately Gauss distributed with the same mean and variance in light of the central limit theorem. In the case of mean zero and variance $\sigma^2$, the magnitude $G = |g(t)|$ has a Rayleigh distribution with the probability density function (PDF) given by

$$p_G(x) = \frac{x}{\sigma^2}\exp\left\{-\frac{x^2}{2\sigma^2}\right\},\ x \geq 0. \tag{1.50}$$

Denote $\mathrm{E}\{\cdot\}$ as the expectation. The average envelope power is given by

$$C_P = \mathrm{E}\left\{G^2\right\} = \mathrm{E}\left\{|g_I(t)|^2 + |g_Q(t)|^2\right\} = 2\sigma^2. \tag{1.51}$$

This type of fading with PDF in (1.50) is called Rayleigh fading. If the means of $g_I(t)$ or $g_Q(t)$ are nonzero and denoted by $\mu_I$ and $\mu_Q$, respectively, then $G$ is Ricean distributed or

$$p_G(x) = \frac{x}{\sigma^2}\exp\left\{-\frac{x^2+\mu^2}{2\sigma^2}\right\}\mathrm{I}_0\left(\frac{\mu x}{\sigma^2}\right) \tag{1.52}$$

for $x \geq 0$ where $\mu^2 = \mu_I^2 + \mu_Q^2$ and

$$\mathrm{I}_0(x) := \frac{1}{2\pi}\int_0^{2\pi} e^{x\cos(\theta)}\,\mathrm{d}\theta \tag{1.53}$$

is the zero-order modified Bessel function of the first kind. The type of fading as described in (1.52) is called Ricean fading.

Rayleigh and Ricean fading channels are common when line of sight (LoS) exists between the transmitter and receiver. On the other hand, complete obstructions often result in log-normal fading channels in which $\ln(G)$ is normal distributed. Another widely used channel is Nakagami fading in which the magnitude of the received envelope is described by the PDF

$$p_G(x) = \frac{2m^m x^{2m-1}}{\Gamma(m)C_P^m}\exp\left\{-\frac{mx^2}{C_P}\right\},\ m \geq \frac{1}{2}, \tag{1.54}$$

where $\Gamma(\cdot)$ is the Gamma function satisfying

$$\Gamma(x) = \int_0^\infty u^{x-1}e^{-u}\,\mathrm{d}u \tag{1.55}$$

that reduces to $n!$, if $x = n$ is an integer.

Nakagami fading is more versatile. In the case of $m = 1$, Nakagami distribution becomes Rayleigh distribution. For $m > 1$, it provides a close approximation to Ricean fading by taking

$$m = \frac{(K+1)^2}{2K+1} \iff K = \frac{\sqrt{m^2-m}}{m-\sqrt{m^2-m}}, \tag{1.56}$$

where $K = \frac{\mu^2}{2\sigma^2}$ is called Rice factor and $\Longleftrightarrow$ stands for "equivalence." In the case of $m \to \infty$ or $K \to \infty$, the PDF approaches an impulse, and thus, the channel experiences no fading at all.

Recall that flat fading is associated with large $T_\mathrm{s}$ that is the duration of the modulated symbol. Since continuous-time waveforms are low-pass, the transmitted signal has narrowband if $T_\mathrm{s}$ is considerably greater than multipath delay spreads.

However, as $T_s$ decreases, signal bandwidth increases. In the case of wide band signals, the frequency components in the transmitted signal experiences different phase shifts along the different paths. Under this condition, the channel introduces both magnitude and phase distortion into the message waveform. Such a channel exhibits *frequency-selective fading*.

When delay spreads are considerable greater than the symbol duration, the impulse response in (1.45) cannot be approximated as in (1.47). Instead, it is more conveniently represented by

$$g(t;\tau) = \sum_{k=1}^{N} g_k(t)\delta_D(\tau - d_k), \tag{1.57}$$

where $g_k(t) = C_k e^{-j[\omega_{D,k}d_k - \omega_c(t-d_k)]}$. Experimental tests show uncorrelated scattering (US) in the sense that $\{g_k(t)\}$ are uncorrelated for all time $t$. In addition, each path gain $g_k(t)$ is wide-sense stationary (WSS), i.e.,

$$R_{g_k}(t,\tau) = \mathrm{E}\{g_k(t)\bar{g}_k(\tau)\} = R_{g_k}(t-\tau), \tag{1.58}$$

with $\bar{\cdot}$ for complex conjugation. While wide-sense stationary and uncorrelated scattering (WSSUS) channels are very special, many radio channels satisfy the WSSUS assumption.

The wireless channels discussed thus far involve only single transmit/receive antenna. More and more mobile radio systems nowadays begin to employ antenna diversity by using multiple spatially separated antennas at both the transmitter and the receiver which result in MIMO channels. These antennas provide multiple faded replica of the same information bearing signal thereby increasing the channel capacity. The impulse response for the MIMO channel has the similar form as in (1.57), but the scalar path gain $g_k(t)$ is now replaced by the matrix function $G_k(t)$ of size $P \times M$, assuming $M$ antennas at the transmitter and $P$ antennas at the receiver, yielding the impulse response

$$G(t;\tau) = \sum_{k=1}^{N} G_k(t)\delta_D(\tau - d_k). \tag{1.59}$$

It is important to note that the impulse responses in (1.57) and (1.59) describe the channels in continuous time. Channel discretization will have to be carried out prior to processing the digital data which will be studied in the next subsection.

### *1.2.2 Channel Discretization*

One of the fundamental issues in data communications is retrieval of the transmitted data at the receiver. Consider the schematic block diagram shown in Fig. 1.5.

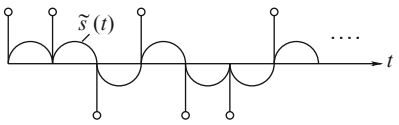


**Fig. 1.6** A typical binary data signal and its associated waveform

At the transmitter site, the data are coded, modulated, and frequency shaped by the continuous-time waveform, and then sent through the channel. The transmitted signal experiences random distortion in the channel Ch due to various fading phenomena. At the receiver site, the observed noisy signal is processed, demodulated, and decoded by the receiver, in hope of recovering the original data.

The channel is a physical entity that cannot be altered by designers, even though no physical devices exist for channels in the case of wireless communications. In the case of wide band signals, the channel experiences frequency-selective fading. If channel distortions are function of time, then the channel experiences *time-selective* fading. Channel fading is one of the main impediments to data communications. In contrast to the channel, the transmitter and receiver can be altered by designers. For simplicity, it is assumed that both the transmitter and the receiver are linear. The nonlinear effects of modulation and codings are omitted, in order for us to focus on the basic issues in data communication. An objective of this text is design of wireless transceivers, i.e., the transmitters and receivers, to detect the transmitted data at the output of the receiver with the minimum achievable error probability.

The simplest data set consists of binary symbol of $\pm 1$. Let $\{b(k)\}$ be coded and binary valued data. The transmitted signal shown in Fig. 1.5 is continuous and has the form of:

$$\tilde{s}(t) = \sum_{k=-\infty}^{\infty} b(k)\psi(t - kT_s), \tag{1.60}$$

where $\psi(\cdot)$ is the continuous-time waveform with support $[0,\ T_s]$ and $T_s > 0$ is the symbol period. Typical $\psi(\cdot)$ includes sinusoidal and rectangular functions (see Fig. 1.6).

Let $g(t;\tau)$ be the channel impulse response (CIR) in (1.45). The physical nature of the channel implies causality of $g(t;\tau)$, i.e., $g(t;\tau) = 0$ for $\tau < 0$. It follows that

$$\begin{aligned} \tilde{r}(t) &= \int_{-\infty}^{t} g(t;t-\tau)\tilde{s}(\tau)\,\mathrm{d}\tau + \eta(t) \\ &= \sum_{k=-\infty}^{\infty} b(k) \int_{-\infty}^{t} g(t;t-\tau)\psi(\tau - kT_s)\,\mathrm{d}\tau + \eta(t) \end{aligned} \tag{1.61}$$

is the signal at the receiver with $\eta(t)$ additive noises. For wireless communication systems with high data rate, $T_s$ is rather small, and thus,

$$g(t;\tau) \approx \sum_{i=0}^{L_h-1} h_i(t)\delta_D(\tau - \tau_i), \tag{1.62}$$

where $0 \le \tau_0 < \tau_1 < \cdots < \tau_{L_h-1}$. The change of notation from (1.57) is due to possible regrouping of those terms with delay spreads close to each other.

It is easy to see that $\tau_i = (\ell_i + \varepsilon_i)T_\mathrm{s}$ for some integer $\ell_i$ and $\varepsilon_i \in [0,\ 1)$. Upon substituting (1.62) into (1.61) yields:

$$\tilde{r}(t) = \sum_{k=-\infty}^{\infty} b(k) \sum_{i=0}^{L_h-1} h_i(t)\psi(t-(\ell_i+k)T_\mathrm{s}-\varepsilon_i T_\mathrm{s}) + \eta(t). \tag{1.63}$$

In order to recover the digital data $\{b(k)\}$, a common approach applies the matched filter to $\tilde{r}(t)$. Assume that $h_i(t) \approx h_i(n)$ over $[nT_\mathrm{s}, (n+1)T_\mathrm{s})$, by an abuse of notation and the fact of small $T_\mathrm{s}$ due to high data rate. Thus

$$y(n) = \int_{nT_\mathrm{s}}^{(n+1)T_\mathrm{s}} \tilde{r}(t)\psi(t-nT_\mathrm{s})\,\mathrm{d}t = \sum_{k=-\infty}^{\infty} b(k) \sum_{i=0}^{L_h-1} h_i(n)J_i(n) + v(n) \tag{1.64}$$

with $J_i(n)$ the $i$th integral given by

$$J_i(n) = \int_{nT_\mathrm{s}}^{(n+1)T_\mathrm{s}} \psi(t-(\ell_i+k)T_\mathrm{s}-\varepsilon_i T_\mathrm{s})\psi(t-nT_\mathrm{s})\,\mathrm{d}t,$$

and $v(n)$ the integral of $\psi(t-nT_\mathrm{s})\eta(t)$ over $[nT_\mathrm{s}, (n+1)T_\mathrm{s}]$.

Denote $\delta_k$ as the Kroneker delta function specified by

$$\delta_k = \begin{cases} 1, & \text{if } k = 0, \\ 0, & \text{otherwise.} \end{cases}$$

It can be verified that the integral $J_i(n)$ admits the expression

$$\begin{aligned} J_i(n) &= \delta_{n-k-\ell_i} \int_{\varepsilon_i T_\mathrm{s}}^{T_\mathrm{s}} \psi(\tau-\varepsilon_i T_\mathrm{s})\psi(\tau)\,\mathrm{d}\tau \\ &\qquad + \delta_{n-k-\ell_i-1} \int_0^{\varepsilon_i T_\mathrm{s}} \psi(\tau+(1-\varepsilon_i)T_\mathrm{s})\psi(\tau)\,\mathrm{d}\tau \\ &= \alpha_i(n)\delta_{n-k-\ell_i} + \beta_i(n)\delta_{n-k-\ell_i-1}. \end{aligned}$$

Substituting the above into (1.64) yields

$$\begin{aligned} y(n) &= \sum_{k=-\infty}^{\infty} b(k) \sum_{i=0}^{L_h-1} h_i(n)[\alpha_i(n)\delta_{n-k-\ell_i} + \beta_i(n)\delta_{n-k-\ell_i-1}] + v(n) \\ &= \sum_{i=0}^{L_h-1} h_i(n)[\alpha_i(n)b(n-\ell_i) + \beta_i(n)b(n-\ell_i-1)] + v(n). \end{aligned}$$

Let $L = 1 + \max\{\ell_i : 0 \le i < L\}$. Then

$$y(n) = \sum_{k=0}^{L} \phi(n;k) b(n-k) + v(n), \tag{1.65}$$

where $\phi(n;k)$ is the impulse response of the discretized channel at time index $n$ and depends on $\{\alpha_i(n)\}$, $\{\beta_i(n)\}$, and $\{h_i(n)\}$. See Problem 1.16 in Exercises. In the MIMO case, the discretized CIR consists of matrices $\Phi(n;k)$. Both input and output are vector-valued, denoted by $\mathbf{b}(n)$, $\mathbf{v}(n)$, and $\mathbf{y}(n)$, respectively, leading to dynamic equation of

$$\mathbf{y}(n) = \sum_{k=0}^{L} \Phi(n;k) \mathbf{b}(n-k) + \mathbf{v}(n).$$

Generically, the wireless channel has the form of transversal filters. This fact is attributed to the finite duration of the CIR for wireless channels, contrast to the plant model in control systems.

## 1.3 Organization of the Book

This textbook is aimed at presentation of theory and design of linear discrete-time systems with applications to feedback control systems and wireless transceivers, although the primary audience is from the control area. This book probably represents the first attempt to present feedback control systems and wireless communication systems together, motivated by MIMO and linearity of the underlying dynamic systems. The author believes that readers from these two different areas will learn more by showing them new perspectives in linear systems. The book begins with warm-up examples and discretization in Chap. 1. Various signal and system models are introduced in Chap. 2. The core materials are Chaps. 3 and 5 in which the main results in linear system theory and optimal control/filtering are presented. These two are the most important chapters and are also the most theoretic part of this text. Chapter 4 is concerned with model reduction that is more oriented to feedback control systems. Compared with undergraduate control textbooks, this text clearly has more mathematical depth. The main reason lies in the MIMO nature of the modern control systems that are difficult to analyze and control. Chapters 3 and 5 provide mathematical notions and theory for us to understand MIMO linear systems.

While most textbooks on linear systems are focused on theory, this textbook makes an effort to present design, that is a tremendous challenge. Chapter 6 considers design of feedback control systems, while Chap. 7 is focused on design of wireless transceivers in data communications. Although the author wishes to present the state-of-art design techniques, these two chapters may not fulfill this wish. Design is not science. Various objectives arising from engineering practice are difficult to be modeled by a single performance index, and minimization of

some mathematical functional may not lead to the desired feedback control system. However, the author hopes that Chap. 6 provides some guidelines for readers to learn design of MIMO feedback control systems, and Chap. 7 provides some mathematical tools for design of wireless transceivers. Chapter 8 is the final chapter that is aimed at modeling and identification of linear systems. It helps readers to know where the linear models come from and how to obtain them given input and output measurements of the MIMO systems. The textbook also includes three appendix chapters that are aimed at helping readers to prepare their mathematical background.

This book can be used as a textbook for the first and second year graduate students, although sophisticated senior students can also be the audience. It can be used either for one semester or for two semesters, dependent on the curriculum. If the book is used as a textbook for one semester, then the author suggests to focus on Chaps. 1–3, and 5. The instructors can use related material from other chapters as supplements. For instance, a class oriented to control may wish to use the control system design material from Chaps. 4 and 6, while a class oriented to DSP may wish to use the wireless transceiver design material from Chaps. 7 and 8. However, if a second semester is needed, then Chaps. 4, 6–8 can be taught together with suitable design projects. The author has taught several times at LSU as a one semester course, tested with different focuses, which result in this textbook. Many control students like the course that helps to diversify their background and to seek jobs in wireless communications and DSP. Indeed, many of them, including my own students, have taken other courses in digital and wireless communications afterward, and are currently working in high-tech companies such as Qualcomm, Broadcom, etc. Their control background actually helps them to do well in their new careers which is also one of the motivations for the author to write this textbook.

Each chapter of this book has a section of exercises. Problems in these exercise sections are carefully designed to help readers get familiar with the new concepts and knowledge presented in the main text. Some of the problems are part of the topics studied in different chapters. The author hopes that this will help readers study the material more actively. Some of the problems can be very hard. A solution manual will be worked out to aid instructors and readers in the future.

## Notes and References

Discretization of continuous-time signals and systems are covered by many books. See for instance [23, 73, 90] and [64, 83–85]. The flight control example can be found in [80, 81]. The modeling of inverted pendulum employs the principle from Lagrange mechanics [17, 108]. For discretization and modeling of wireless communication channels, many papers and books are available. The books [19, 98, 107, 111] are recommended for further reading.

## Exercises

**1.1.** For the inverted pendulum as described in (1.6) and (1.5), assume that the control force is generated by the actuator via

$$u(t) = \frac{K}{Rr}\left[u_{\text{in}}(t) - \frac{K}{r}\dot{p}(t)\right],\ K = K_m K_g. \tag{1.66}$$

The above is a simple model for DC motor with $u_{\text{in}}(t)$ as the armature voltage. Show that the dynamic system is now described by

$$\ddot{\theta} = \frac{mL}{\Delta}\left(\frac{K\cos(\theta)}{Rr}u_{\text{in}} + (M+m)g\sin(\theta) - \frac{mL\sin(2\theta)}{2}\dot{\theta}^2 - \frac{K^2\cos(\theta)}{Rr^2}\dot{p}\right),$$
$$\ddot{p} = \frac{mL}{\Delta}\left(\frac{K}{Rr}u_{\text{in}}(t) + \frac{mg\sin(2\theta)}{2} - mL\sin(\theta)\dot{\theta} - \frac{K^2}{Rr^2}\dot{p}\right),$$

where $\Delta = \left(M + m\sin^2(\theta)\right)mL^2$.

**1.2.** For the nonlinear ODE in Problem 1.1, assume that $\theta$ and $p$ are output measurements. Denote $\mathbf{x}(t)$ in (1.7) as the state vector. Show that its linearized system has realization matrices $(A,B,C,D)$ given by

$$A = \begin{bmatrix} 0 & 1 & 0 & 0 \\ \frac{(M+m)g}{ML} & 0 & 0 & -\frac{K^2}{Rr^2} \\ 0 & 0 & 0 & 1 \\ \frac{mg}{M} & 0 & 0 & -\frac{K^2}{Rr^2} \end{bmatrix},\quad B = \begin{bmatrix} 0 \\ \frac{K}{MLRr} \\ 0 \\ \frac{K}{MRr} \end{bmatrix},$$
$$C = \begin{bmatrix} 1 & 0 & 0 & 0 \\ 0 & 1 & 0 & 0 \end{bmatrix},\qquad D = \begin{bmatrix} 0 \\ 0 \end{bmatrix}.$$

**1.3.** Use Matlab Simulink toolbox to simulate the controlled pendulum system in Example 1.1 by using parameters

$$K_{dy} = -524.4300,\ z_y = 0.8200,$$
$$K_{d\theta} = 334.2439,\ z_\theta = 6.2589,$$

and $p_d = 14.9672$.

**1.4.** For Dirac delta function defined in (1.16), show that

$$\int_{-\infty}^{\infty} f(t)\delta_D(t-\tau)\,\mathrm{d}t = f(\tau)$$

for any function $f(t)$ that is continuous at $t = \tau$. In addition, show that the periodic Dirac delta function with period $T$ satisfies

$$p_\delta(t) = \sum_{k=-\infty}^{\infty} \delta_D(t - kT) = \frac{1}{T} \sum_{i=-\infty}^{\infty} \mathrm{e}^{ji\omega t},$$

where $\omega = 2\pi/T$.

**1.5.** Prove the CTFT for $s_p(t)$ in (1.21).

**1.6.** Prove Lemma 1.2 by first finding the impulse to the zero-order holder and then its CTFT.

**1.7.** Verify the expression in (1.40) for BT-based discretization.

**1.8.** Show that under the SIT discretization, the frequency response error between the continuous-time transfer function $G(s)$ and the discretized transfer function $G_d(z)$ is given by

$$\left|G(j\omega) - G_d\left(\mathrm{e}^{j\omega}\right)\right| = \left|G(j\omega)\left[R(j\omega) - 1\right]\right|,$$

where $R(s) = \left(1 - e^{-sT_\mathrm{s}}\right)/s$, provided that the cutoff frequency of $G(s)$ is smaller than half of the sampling frequency.

**1.9.** Suppose that $A$ has eigenvalues at $0, 0, \pm j, 1 \pm 2j$. Show that the pathological sampling frequency $\omega_\mathrm{s}$ is in the set of $\left\{\frac{4}{k} : k \text{ integers}\right\}$.

**1.10.** For the inverted pendulum plant model in (1.11) and (1.10), do the following:

(i) Discretize $G_{up}(s)$ and $G_{u\theta}(s)$ with sampling frequency $f_\mathrm{s} = 10\,\mathrm{Hz}$.
(ii) Discretize the above transfer functions with one sampling frequency $f_\mathrm{s} < 10$ and the other $f_\mathrm{s} > 10$.
(iii) Recommend one sampling frequency and detail your reason. In addition, make frequency domain analysis for the sampling frequency you recommend.

(*Note:* Matlab command "c2d" can be used to discretize the plant.)

**1.11.** Consider a flight control system with 3-input/3-output. This model is linearized from an aircraft motion in the vertical plane when small perturbations about a flight condition are considered. The linearized model is described by state-space realization given by

$$A = \begin{bmatrix} 0 & 0 & 1.132 & 0 & -1 \\ 0 & -0.0538 & -0.1712 & 0 & 0.0705 \\ 0 & 0 & 0 & 1 & 0 \\ 0 & 0.0485 & 0 & -0.8556 & -1.013 \\ 0 & -0.2909 & 0 & 1.0532 & -0.6859 \end{bmatrix},$$

$$B = \begin{bmatrix} 0 & 0 & 0 \\ -0.0012 & 1 & 0 \\ 0 & 0 & 0 \\ 0.4419 & 0 & -1.6646 \\ 0.1575 & 0 & -0.0732 \end{bmatrix}, \quad C = \begin{bmatrix} 1\,0\,0\,0\,0 \\ 0\,1\,0\,0\,0 \\ 0\,0\,1\,0\,0 \end{bmatrix}.$$

Repeat (i)–(iii) in the previous problem except that 10 Hz is replaced by 20 Hz, plus zero/pole plots.

**1.12.** For the time-varying impulse response in (1.45), show that the output response due to input $\tilde{s}(t)$ is given in (1.44).

**1.13.** For $r(t)$ in (1.48), assume that $r(t)$ is WSS, $\{\omega_{D,k}\}$ are identically distributed, and $\{\phi_k(t)\}$ are independent and uniformly distributed over $[-\pi, \pi]$. Show that

$$R_r(\tau) = \mathrm{E}[r(t)r(t+\tau)] = A(\tau)\cos(\omega_c\tau) - B(\tau)\sin(\omega_c\tau),$$

where expectation is taken for $V_k = \omega_c d_k$ which is uniformly distributed over $[-\pi,\ \pi]$ and for the Doppler frequency. The expressions of $A(\tau)$ and $B(\tau)$ are given by

$$A(\tau) = C_P\mathrm{E}[\cos(\omega_{D,k}\tau)],\ B(\tau) = C_P\mathrm{E}[\sin(\omega_{D,k}\tau)],$$

with expectation taken for only the Doppler frequency and $C_P$ as in (1.51).

**1.14.** Suppose that $X_1$ and $X_2$ are independent Gauss with zero mean and common variance $\sigma^2$. Let

$$G = \sqrt{X_1^2 + X_2^2},\ P = \tan^{-1}(X_2/X_1). \tag{1.67}$$

Show that $G$ is Rayleigh distributed as in (1.50) and $P$ is uniformly distributed.

**1.15.** Consider the same $X_1$ and $X_2$ as in the previous problem except that $\mathrm{E}\{X_1\} = \mu_1$ and $\mathrm{E}\{X_2\} = \mu_2$. Define $G$ and $P$ as in (1.67), and $t = \tan^{-1}(\mu_2/\mu_1)$. Let $\mu = \sqrt{\mu_1^2 + \mu_2^2}$. Show that

$$p_{RP}(r,p) = \frac{r}{2\pi\sigma^2}\exp\left\{-\frac{r^2+\mu^2-2r\mu\cos(p-t)}{2\sigma^2}\right\}$$

and then verify the Ricean PDF in (1.52) using

$$p_R(r) = \int_0^{2\pi} p_{RP}(r,p)\,\mathrm{d}p.$$

**1.16.** Find the expression of $\phi_i(n;k)$ in (1.65) in terms of $\{\alpha_i(n)\}$, $\{\beta_i(n)\}$, and $\{h_i(n)\}$, assuming $\ell_i = i$ for each $i$.